ACS OMEGA

http://pubs.acs.org/journal/acsodf

Article

Preparation and Characterization of Antibacterial Porcine Acellular Dermal Matrices with High Performance

Lu Wang, Juxia Gong, Ye Dan, Yanping Huang, Nianhua Dan,* and Weihua Dan*

Cite This: *ACS Omega* 2020, 5, 20238−20249

Read Online

ACCESS | Metrics & More | Article Recommendations

ABSTRACT: Infection is a common complication in the process of wound management. An ideal wound dressing is supposed to reduce or even prevent the infection while promoting wound healing. A porcine acellular dermal matrix (pADM) has been already used as a wound dressing in clinic due to its capacity to accelerate wound healing. However, not only is pure pADM not antibacterial, its mechanical properties are poor. In this study, an antibacterial pADM with good performance was prepared by adding two natural products as modifiers, quercetin (QCT) and tea tree oil (TTO). The result of Fourier-transform infrared (FTIR) proved that the addition of modifiers did not break the natural triple-helical structure of collagen. Meanwhile, the results of differential scanning calorimetry (DSC), thermogravimetric analysis (TG), mechanic experiment, and enzymatic degradation demonstrated that pADM handled with QCT and TTO (termed QCT−TTO−pADM) had better thermal stability, mechanical strength, and resistance to enzymatic degradation than pADM. Meanwhile, QCT−TTO−pADM had excellent antibacterial activity and showed an antibacterial rate of over 80%. Furthermore, in the cytocompatibility analysis, QCT−TTO−pADM had no side effects on the adhesion, growth, and proliferation of fibroblasts. QCT−TTO−pADM could even accelerate wound healing more efficiently than pADM and glutaraldehyde-modified pADM (GA-pADM). In conclusion, QCT−TTO−pADM was a potential antibacterial wound dressing with good performance.

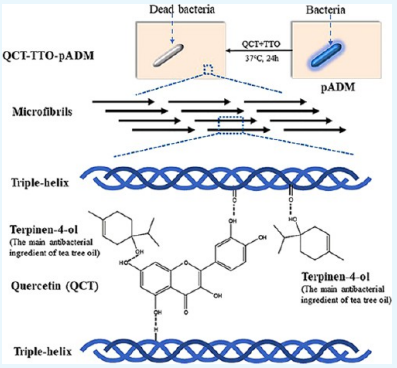

1. INTRODUCTION

Wound infection is the most common and most influential serious problem after trauma, which not only causes sepsis, amputation, and other adverse complications but also leads to death in severe cases. There are often fragments of tissue, dirt, hair, and necrotic tissue in traumatic wounds, which can lead to an increased and prolonged wound inflammatory response, even secondary infection, and ultimately delayed wound repair.[1] After wound cleansing, debridement, and evaluation, it is particularly important to choose suitable anti-infective wound dressings. So far, the dressings used for local anti-infection in the world mainly include silver-containing dressings, chitosan-based dressings, medical honey dressings, etc., each of which has its limitations. Silver ions have a broad spectrum of antibacterial properties. Many commercial wound dressings containing Ag^+ and its compounds have been developed, such as hydrophilic fiber dressing Aquacel AG. But silver ions may be toxic, causing structural damage to the mitochondria and inducing DNA mutations.[2] Chitosan-based dressings also have broad-spectrum antibacterial properties and good biocompatibility, promoting healing and other physiological activities. Many types of chitosan-based antibacterial dressings have been developed, such as sponges and hydrogels. However, their antibacterial activity is a little bit low, and their molding properties and mechanical properties still need to be improved. Natural antibacterial agents, such as propolis and plant agents, can effectively avoid drug resistance and toxicity and are worth further study.[3] Herein, the bioactive porcine acellular dermal matrix (pADM) was modified with natural antibacterial agents to achieve the dual purpose of wound repair and anti-infection.

pADM, mainly comprised by type I collagen, is widely used as a biomaterial with favorable bioactivity, low antigenicity, and good biocompatibility. Pabst et al. analyzed the influence of pADM on endothelial progenitor cells (EPC) in vitro.[4] The result showed that pADM had good biocompatibility with EPC without any toxicity, which was available for efficient revascularization.[4] The porcine small-intestinal submucosa (SIS) scaffolds were found to promote the attachment, proliferation, and differentiation of mesenchymal stem cells (MSCs) and human umbilical vein endothelial cells (HUVECs).[5,6] Besides, pADM has been proved to be safe and convenient for in vivo implantation, such as breast reconstruction and artificial vascular transplantation.[7−9]

Received: April 27, 2020
Accepted: July 27, 2020
Published: August 8, 2020

https://dx.doi.org/10.1021/acsomega.0c01940
ACS Omega 2020, 5, 20238−20249

However, pure pADM cannot resist infection, which is common in wound management as a wound dressing.[10,11] Beyond that, pADM is easy to be broken by mechanical stress or be degraded by collagenase in vivo, which might cause some problems. Therefore, it is crucial to develop a high-performance pADM that even prevents the infection while promoting wound healing.

Tea tree oil (TTO), extracted from *Melaleuca alternifolia*, is a natural essential oil with broad-spectrum antimicrobial activity.[12−15] TTO consists of a complex mixture of monoterpenoids, in which terpinen-4-ol contributes largely to sterilizing.[13,16] As a natural antibacterial agent, TTO has been gradually applied in wound healing and skin care, and it shows quite high antimicrobial ability.[17] Sánchez-González et al. developed antimicrobial films by adding bergamot oil, lemon oil, and tea tree oil into hydroxypropyl methylcellulose films separately.[18] The results showed that TTO exhibited the highest antimicrobial activity in all film matrices.[18] The addition of TTO might provide pADM with antibacterial ability, but it does not provide mechanical property.

Cross-linking modification is frequently used to improve the physicochemical properties of pADM.[19−21] However, it causes several side effects sometimes. For example, common chemical cross-linking may introduce impurities, which might lead to decreased biocompatibility and even cytotoxicity.[22] To enhance the mechanical property of wound dressing, some natural agents, extracted from plants, are considered as cross-linking agents to avoid cytotoxicity. It was reported that pADM cross-linked by proanthocyanins had good mechanical properties, improved thermostability, and no obvious cytotoxicity.[23]

Quercetin (QCT) is a kind of flavonoid, which exists in vegetables and other plants in the form of glycosides. QCT has a unique molecular structure, which is similar to that of proanthocyanin, with only one additional O atom at four sites.[24] The special structure of quercetin is in relation to the biological activity, antibacterial effect, oxidation resistance, and so on.[25,26] Research has shown that the heart valve obtained improved the mechanical property, resistance to enzymatic degradation after handling QCT.[27] Meanwhile, the heart valve handled with QCT enhanced cell compatibility and strong anticalcification ability.[28]

There are few reports about quercetin being used as a natural cross-linker to modify pADM. In our study, TTO and QCT were selected to give pADM excellent mechanical and antibacterial properties at the same time. The thermal stability, mechanical property, and antibacterial property of materials were assessed. Besides, the biocompatibility of QCT−TTO−pADM both in vitro and in vivo was compared with pADM and glutaraldehyde-modified pADM (GA-pADM).

2. RESULTS AND DISCUSSION

2.1. Fourier-Transform Infrared (FTIR) Analysis. FTIR was applied to study the chemical functional groups and the microstructure of QCT−TTO−pADM with different QCT contents (Figure 1). For pADM, the absorption peak around 1650 cm^{-1}, which was called amide I, was attributed to the C═O stretching vibration, and it can directly reflect the collagen triple-helix structure.[29] Amide I and amide II (1545 cm^{-1}) bands of collagen could directly reflect the secondary structure of collagen. Amide A band (3410 cm^{-1}) reflected the stretching vibration of the N−H group[30] and hydrogen bonds, which could stabilize the triple-helical structure of collagen.[31,32] Amide B band of 2930 cm^{-1} was attributed to CH_2 asymmetrical stretch.

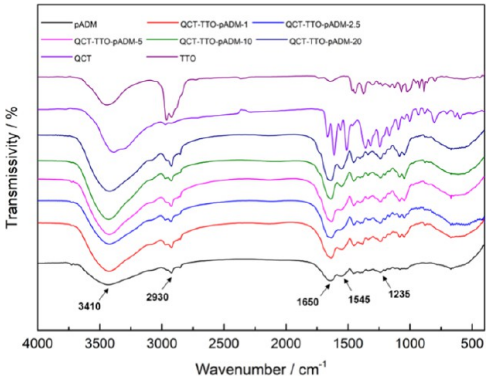

Figure 1. FTIR images of QCT−TTO−pADM with different QCT contents, QCT and TTO.

As shown in Figure 1, the broad region and the enhanced intensity of about 3410 cm^{-1} in the presence of QCT and TTO suggested that the hydrogen bonds might have formed among pADM, QCT, and TTO. Besides, the main characteristic peaks of QCT and TTO in the FTIR spectrum disappeared in QCT−TTO−pADM, suggesting the binding of QCT and TTO to pADM, which could limit their stretching and bending vibrations.[33,34] Amide I band, amide II band, and amide III (1235 cm^{-1}) band, especially the amide I band, could directly reflect the internal arrangement of collagen.[32,35] If the triple-helix structure of collagen was destroyed, all of the characteristic peaks of FTIR would be weakened,[36] and the amide I bands would move to a lower region.[30,35,36] Note that compared with pADM, the amide band, especially the amide I band, barely changed with the change of QCT content,[37] which might suggest that the characteristic triple-helix structure of collagen remains intact after cross-linking modification with QCT and TTO. In addition, the characteristic triple-helix structure is the structural basis of collagen's excellent biological properties.[38] In a way, the addition of QCT and TTO almost had no impact on the biological activity of pADM,[39] coinciding with the consequences of in vitro and in vivo study.

2.2. Thermal Stability Analysis. Thermal denaturation temperature is an important parameter of the collagen-based materials, which can reflect the thermal stability of the materials.[29] pADM is formed by weaving collagen fiber bundles. During the heating process, the intermolecular force is successively reduced. Subsequently, the triple-helix structure of collagen is gradually broken through external heating.

Figure 2A shows the differential scanning calorimetry (DSC) curve of pADM and QCT−TTO−pADM. The denaturation temperature of pADM was 66.7 °C, higher than that of the collagen sponge (54.9 °C).[29] The thermal denaturation temperature of QCT−TTO−pADM gradually increased to 80.2 °C with the increase of the QCT dosage. Collagen peptide chains were constrained by hydrogen bonds, which were formed between catechol groups of QCT and amino groups and hydroxyls group of collagen fibers. In conclusion, the denaturation temperature of the material increased after cross-linking with QCT.

Thermogravimetric analysis (TG) can be used to detect the mass change of QCT−TTO−pADM during heating. As is shown in Figure 2B, the thermal decomposition process of

https://dx.doi.org/10.1021/acsomega.0c01940
ACS Omega 2020, 5, 20238−20249

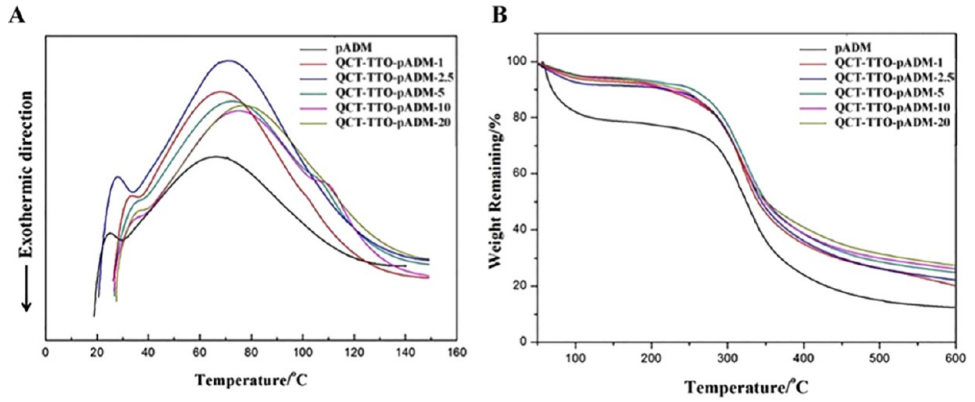

Figure 2. Thermal stability analysis: (A) DSC of QCT−TTO−pADM; (B) TG of QCT−TTO−pADM.

QCT−TTO−pADM was mainly divided into two stages: the water content was decreased at first when the temperature was between 40 and 120 °C. The water loss was caused by the breakage of hydrogen bonds between combined water and the collagen fiber, and hydrogen bonds among the triple-helix structure of collagen.[20] The material loss stage at 120−600 °C was the second stage, mainly caused by the decomposition of the collagen fibers in pADM.[22,40] The mass loss of QCT−TTO−pADM was lower than pADM at 250−500 °C. In addition, the weightlessness rate of QCT−TTO−pADM decreased with the increase of QCT, owing to the formation of the covalent connection between QCT and collagen. After being cross-linked with QCT, the collagen fiber bundle in pADM would become more compact and orderly, eventually leading to a more stable and firmer three-dimensional structure. The results of TG analysis were consistent with the results of DSC in this study. Above all, the QCT−TTO−pADM had high thermal stability and became more difficult to decompose under heat.

2.3. Mechanical Characterization. Tensile strength and elongation at break are important test indexes for the mechanical properties of materials, and are commonly used to characterize the ability of materials to resist external forces. Collagen-based biomedical materials should have a certain flexibility, tensile strength, and tear resistance in clinical application, which affects the wound repair of the body.[20,41] Therefore, it is particularly important to regulate the mechanical properties of collagen-based biomaterials,[41] especially the strength of pADM has been unable to meet clinical needs in some biomedical applications.

Figure 3 shows the test results of tensile strength and elongation at break of pADM cross-linked with different amounts of QCT and TTO. The tensile strength of QCT−TTO−pADM increased initially and then declined gradually with the increase of QCT. This phenomenon also occurred after the QCT cross-linking of a porcine heart valve matrix.[28] When the concentration of QCT was only 5 mg/mL, the tensile strength of QCT−TTO−pADM was about 2.5 times that of the pure pADM. The significant increase of the tensile strength indicated that stable chemical bonds were formed between QCT, TTO, and collagen molecules,[42] making the arrangement of collagen fibers closer, so as to improve the overall tensile strength. Along with the gradual increase of QCT, the tensile strength of QCT−TTO−pADM could reach to 9.9 MPa, higher than that of pADM treated with dehydrothermal treatment and carbodiimide.[20] However, after that, the tensile strength gradually decreased, which may be caused by

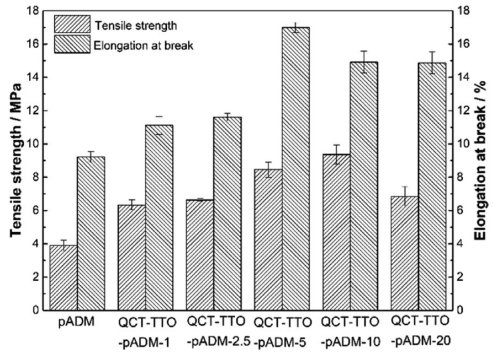

Figure 3. Mechanical characterization of QCT−TTO−pADM.

the complete consumption of reactive groups in pADM and the excessive QCT filling among the fibers, which could disrupt the arrangement of collagen fibers. Its rigid structure was locally too strong, resulting in stress concentration. When subjected to external forces, the collagen fibers in the "tight swelling" state were more likely to fracture.

The proper elongation at break of a collagen-based biomaterial played an important role in supporting the normal morphology and biological function of the tissue in some traumatic body parts that need to maintain tension, such as skin, dura mater, tendon, etc.[43] Compared with pure pADM, the elongation at break of QCT−TTO−pADM was also increased at first and then decreased. pADM is composed of collagen fibers. When the material is deformed by external forces, the tension is not evenly distributed on the collagen fibers. The elongation at break increased at the beginning, probably because of the increase of hydrogen bonds. Unlike covalent bonds, hydrogen bonds are flexible. They could promote the formation of a stable interwoven network between collagen fibers, which made the collagen fibers more resistant to deformation when being stretched by external forces. With the dosage of QCT exceeding 5 mg/mL, the collagen fiber network of QCT−TTO−pADM was woven more closely, forming a tighter and stronger "rigid structure", which mainly leads to a decline in the elongation of the material. When the fiber was stretched, it tended to gather in a directional way, which was more likely to lead to concentrated forces and more difficult to deform, thus reducing the elongation at break.

2.4. Degradation Property Test. Biomedical materials are expected to resist enzyme in vivo so that tissue can recover well before it is completely degraded. For further investigation of the cross-linking effect of QCT on pure pADM, QCT−

https://dx.doi.org/10.1021/acsomega.0c01940
ACS Omega 2020, 5, 20238−20249

TTO−pADM was degraded by type I collagenase, which was specific for collagen degradation and acted directly on the triple-helix structure of collagen. As is shown in Figure 4,

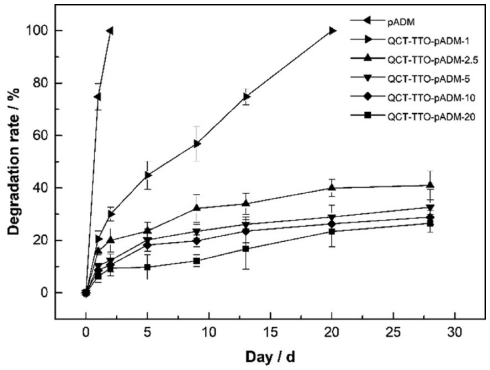

Figure 4. Resistance to the degradation of QCT−TTO−pADM.

pADM was degraded by about 75% in 1 day, and decomposed completely 2 days later. On the contrary, the degradation rate of QCT−TTO−pADM was much lower. After 4 weeks, the QCT−TTO−pADM just degraded by 40%. The result proved that QCT−TTO−pADM could significantly resist the degradation of type I collagenase. This may be attributed to the increase of hydrogen bonds between the hydroxyl groups of QCT and the amino groups of collagen,[28] which made the structure of the collagen microfibers more stable and more difficult for collagenase to degrade.

2.5. Micromorphology Analysis. pADM is a multilevel aggregate composed of collagen molecules, fibrils, fibers, and fiber bundles, with many irregular gaps between the fibers.[29] The new chemical bonds between collagen molecules and fibers could pull the collagen fibers tight, and make the structure of the material contract slightly and become more compact. Figure 5 shows the scanning electron microscope (SEM) images of pADM and QCT−TTO−pADM. It can be seen from Figure 5a that the collagen fiber bundles in pADM were stacked layer by layer and then interwoven together. There were still many gaps interiorly. With the increase of QCT dosage, pADM collagen fiber gaps gradually became smaller, and the material looked more compact. It was obvious that QCT had a significant cross-linking effect on pADM, which was coincident with the results of FTIR, thermal stability analysis, and mechanical characterization.

2.6. Contact Angle (CA) Detection. The surface of biomaterials with good hydrophilicity or moderate hydrophobicity is beneficial to cell adhesion and proliferation.[44,45] The content of adsorbed water in the biofilm mainly depends on the three-dimensional pore structure. Besides, the content of bound water depends on the hydrophilic group of the material.[46] The hydrophilicity of the material was characterized through the surface contact angle test effectively. The lower the CA was, the better the hydrophilicity of the material was. The contact angle of pADM was (113 ± 2)° (Figure 6). The CA

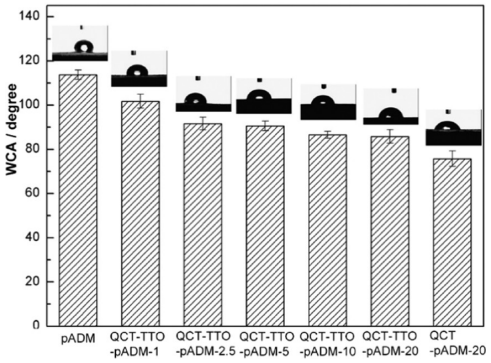

Figure 6. WCA of QCT-pADM films with different dosages of QCT.

reduced in turn after cross-linking, indicating that the hydrophilicity of pADM was significantly improved after cross-linking. The hydroxyl and other hydrophilic groups may be increased with the addition of QCT. Compared with the QCT-pADM, the hydrophilicity of the QCT−TTO−pADM was slightly decreased, owing to that TTO probably brought hydrophobic groups such as hydrocarbon groups. In general, the hydrophilic performance of pADM could still be improved through combined modification of QCT and TTO.

2.7. Antibacterial Properties. Biomedical materials should have antimicrobial properties to prevent wound infection. In this research, TTO, a natural antibacterial agent, was used to provide defenses against bacteria. Figure 7 exhibits

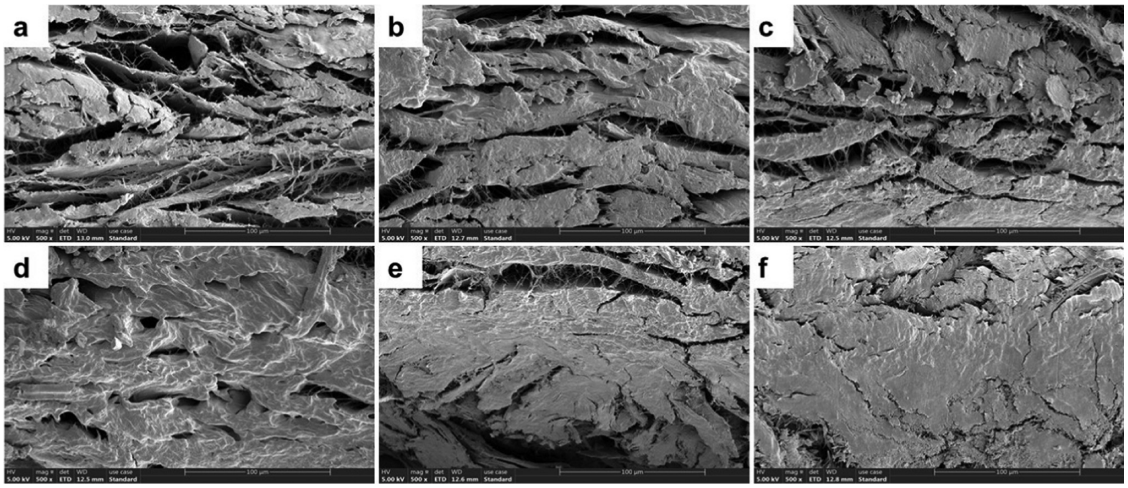

Figure 5. SEM micrographs of QCT−TTO−pADM (×500) (a) pADM, (b) QCT−TTO−pADM-1, (c) QCT−TTO−pADM-2.5, (d) QCT−TTO−pADM-5, (e) QCT−TTO−pADM-10, and (f) QCT−TTO−pADM-20.

https://dx.doi.org/10.1021/acsomega.0c01940
ACS Omega 2020, 5, 20238−20249

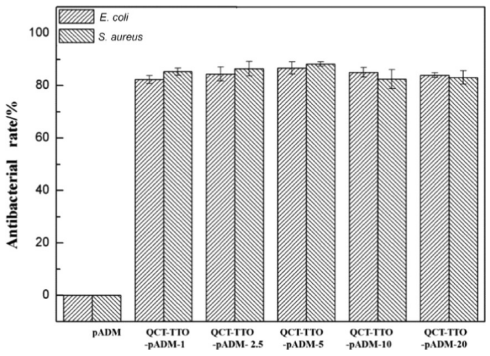

Figure 7. Antibacterial effect of QCT−TTO−pADM against *E. coli* and *S. aureus*.

that the bacteriostatic rate of QCT−TTO−pADM both on *Staphylococcus aureus* and *Escherichia coli* was excellent, which could be up to 80%. Obviously, the introduction of TTO resulted in the high antibacterial rate, and the addition of QCT hardly affected the antibacterial rate. The main bactericidal ingredient, such as terpinen-4-ol, entered into the gaps of pADM, might cross-link with collagen fibers by hydrogen bonds, eventually made pADM antibacterial. Some studies have shown that the TTO components can destroy the bilayer structure of the microbial cell membrane, which resulted in a large release of cell fluid.[47] In addition, some components of TTO could induce bioenzyme to degrade the cell wall, leading to cell autolysis and finally to death.[48] The specific antimicrobial pathways of TTO on pADM deserve further study in future work.

2.8. Cytocompatibility Analysis. The 3-(4,5-Dimethylthiazol-2-yl)-2,5-diphenyltetrazolium bromide (MTT) method is often used to evaluate cell survival and proliferation in vitro. The succinate dehydrogenase of the mitochondria in living cells can reduce MTT to form formazan, a blue-purple crystal insoluble in water. No succinate dehydrogenase can form formazan in dead cells. Thus, the mass of formazan is proportional to the number of living cells.[49] The absorbance of the dimethyl sulfoxide solution with formazan is determined by microplate microscopy. The cytotoxicity of QCT−TTO−pADM is determined by an MTT assay. In this study, mouse L929 cells were cultured in the QCT−TTO−pADM extract with different dosages for 1, 3, and 5 days by the MTT method. The optical density (OD) values of all of the cells on the materials increased (Figure 8A), indicating that cells were proliferating normally. At the same time, the relative growth rate (RGR) of cells showed a declining trend with the addition of QCT, but the RGR still remained higher than 75%. Type I collagen was the main component of pADM, which contributed greatly to cell adhesion, growth, and proliferation. It could be seen from Figure 8B that the fibroblast was in a good growth state with a long spindle shape. It turned out that QCT−TTO−pADM had weak cytotoxicity, meeting the requirements of biomaterials for cellular compatibility.

2.9. Cell Affinity and Wound Healing. When the concentration of QCT was 5 mg/mL, the QCT−TTO−pADM was flexible enough while maintaining high strength and a high antibacterial rate. This antibacterial dressing with high strength and flexibility had the potential for some specific clinical applications. To verify its ability to promote wound repair and prevent infection, the biocompatibility of pADM, QCT−TTO−pADM, and pADM treated with 5% glutaraldehyde (GA-pADM) was investigated. The animal model of skin trauma in Sprague Dawley rats (SD rats) was selected to investigate the effect between QCT−TTO−pADM (cross-linked pADM when the concentration of QCT was 5 mg/mL) and wound through wound healing observation, histology observation, and immunohistochemical analysis.[50]

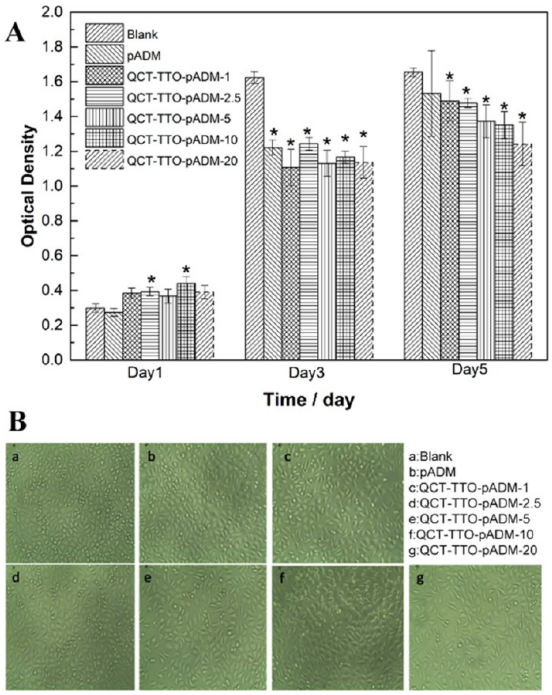

Figure 8. (A) Proliferation of L929 fibroblasts cultured in the extraction liquid of pADM and QCT−TTO−pADM; (B) morphology images of L929 fibroblasts for 3 days.

Figure 9 shows the wound healing observation and wound residual area of the three groups. After 1 week, the wound contraction of the three groups decreased. The wound residual area of QCT−TTO−pADM group even reduced by 65%, much faster than other groups. There was no obvious exudation and pus around the wound, which was only covered with some blood scab. After 2 weeks, the wound area of each group was further reduced. The wound in group c was already very small, and the unhealed area was accounted for 23.41 ± 4.57% of that at the beginning.[51] However, the residual wound areas in groups a, b, and the blank control group were still more than 50%. Three weeks later, the wounds in each group healed well. The wound handled with QCT−TTO−pADM approached complete healing. The skin color was close to the surrounding healthy skin, but there was almost no hair growth.[52] It could be observed visually that QCT−TTO−pADM had good biocompatibility and had positive influence on wound healing of full-thickness skin defect on SD rats.

Figures 10 and 11 show the haematoxylin−eosin staining (HE) and Masson staining of the blank control group and three groups of materials for repairing full-thickness skin defects in SD rats. It can be seen from the figures, typical granulation tissue appeared in each group, with fibroblasts and capillaries emerging in the first week. There were fewer inflammatory cells in trauma. In group a, the wound structure was loose, disordered, and had fewer regenerated collagen fibers. However, dense collagen could be seen in the other three groups. After 2 weeks, the wound area had fewer inflammatory cells and more capillaries and collagen fibers.

https://dx.doi.org/10.1021/acsomega.0c01940
ACS Omega 2020, 5, 20238−20249

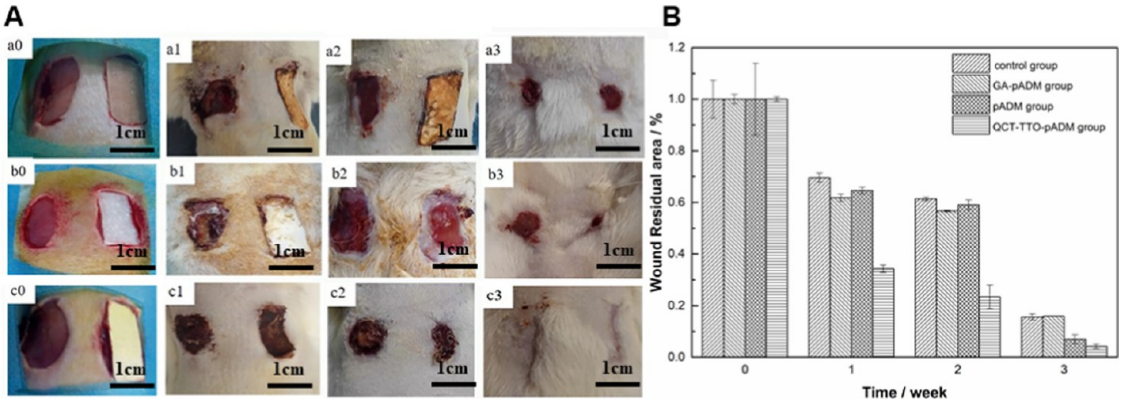

Figure 9. (A) Image of the wound treated with materials (a) GA-pADM group, (b) pADM group, (c) QCT−TTO−pADM group; (a0, b0, c0) 0 week; (a1, b1, c1) 1 week; (a2, b2, c2) 2 weeks; (a3, b3, c3) 3 weeks and (B) quantification of the wound residual area.

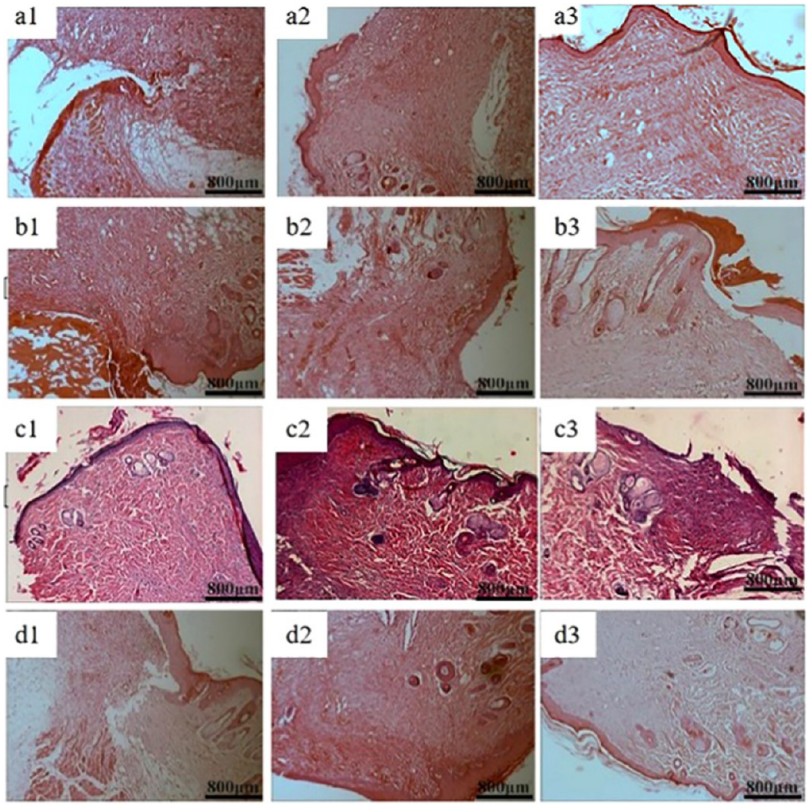

Figure 10. HE staining of wound areas treated with four kinds collagen-based scaffolds (a) blank group, (b) GA-pADM group, (c) pADM group, (d) QCT−TTO−pADM group; (a1, b1, c1, d1) 1 week; (a2, b2, c2, d2) 2 weeks; (a3, b3, c3, d3) 3 weeks.

The fiber bundles in the area became thicker and intertwined into a network. At the same time, the proliferation of epidermis cells and keratinocytes around the wound promoted the formation of the epidermis. The collagen fibers in QCT−TTO−pADM group were more compact by contrast. After 3 weeks, the formation of the epithelium in QCT−TTO−pADM group was more robust than that of the blank, while the collagen fibrils of the GA-pADM group were looser.[53] In QCT−TTO−pADM group, the surface layer of new-born skin was thicker and the weaving of dermis fibers was closer than others. Overall, QCT−TTO−pADM demonstrated high-efficiency in wound healing.

The wound healing process of the body is complex. The ability of healing, neovascularization, and regeneration of each material can be reflected by the specific expression of a vascular endothelial growth factor (VEGF), a platelet-derived growth factor (PDGF), and a basic fibroblast growth factor (bFGF) in the process of skin wound healing.[54,55]

Figures 12 and 13 show VEGF, PDGF, and bFGF immunohistology results of three groups of materials for repairing full-thickness skin defects in SD rats. After 1 week, the positive expression of VEGF in each group was weak, indicating that VEGF could provide nutrition for granulation tissue and promote capillary formation in the early stage of wound repair.[56] Two weeks later, the positive expression of the growth factor in QCT−TTO−pADM group was significantly higher than that in the blank group[57] and a little higher than that of GA-pADM group and pADM group. QCT−TTO−pADM had good antibacterial property, biocompatibility, and the ability to feedback and regulated the growth of cells and

https://dx.doi.org/10.1021/acsomega.0c01940
ACS Omega 2020, 5, 20238−20249

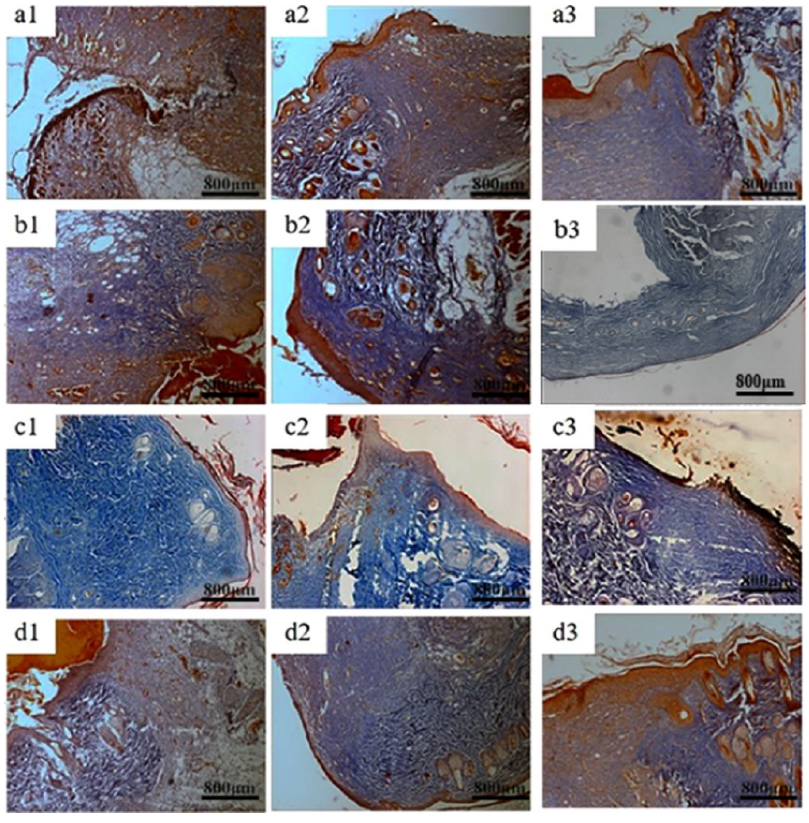

Figure 11. Masson staining of wound areas treated with three kinds collagen-based scaffolds (a) blank group, (b) GA-pADM group, (c) pADM group, (d) QCT−TTO−pADM group; (a1, b1, c1, d1) 1 week; (a2, b2, c2, d2) 2 weeks; (a3, b3, c3, d3) 3 weeks.

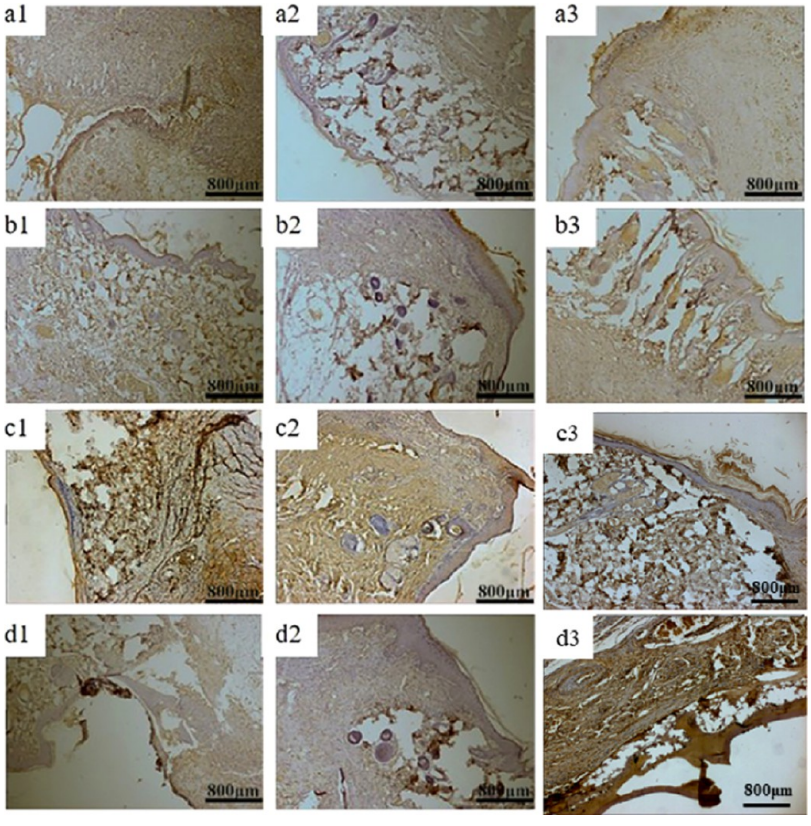

Figure 12. VEGF immunohistochemical analysis of wound areas treated with three kinds collagen-based scaffolds (a) blank group, (b) GA-pADM group, (c) pADM group, (d) QCT−TTO−pADM group; (a1, b1, c1, d1) 1 week; (a2, b2, c2, d2) 2 weeks; (a3, b3, c3, d3) 3 weeks.

https://dx.doi.org/10.1021/acsomega.0c01940
ACS Omega 2020, 5, 20238−20249

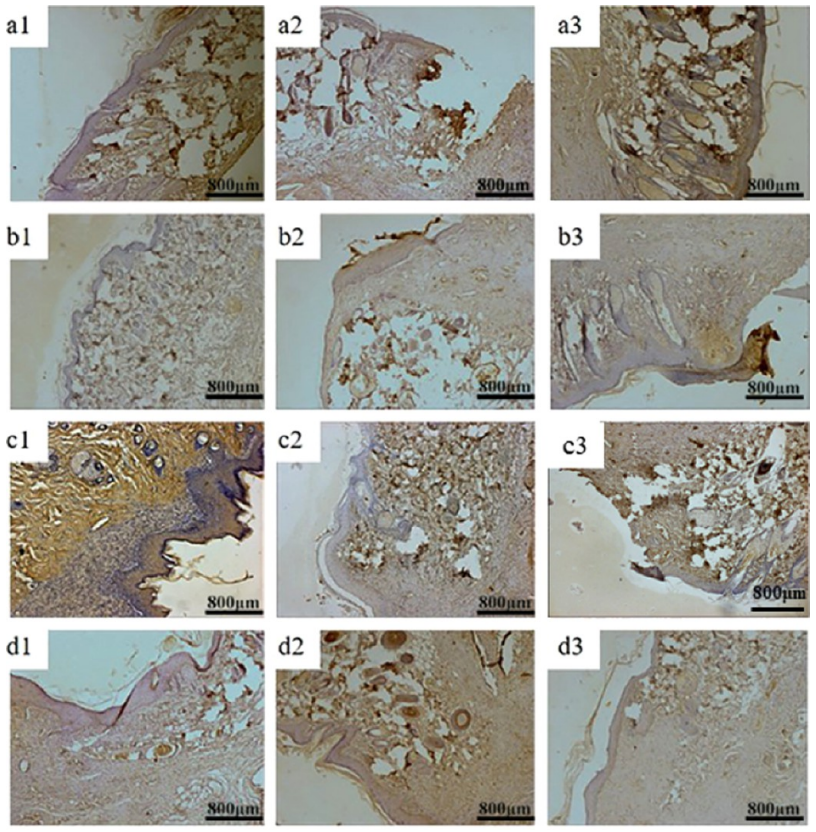

Figure 13. PDGF immunohistochemical analysis of wound areas treated with three kinds collagen-based scaffolds (a) blank group, (b) GA-pADM group, (c) pADM group, (d) QCT−TTO−pADM group; (a1, b1, c1, d1) 1 week; (a2, b2, c2, d2) 2 weeks; (a3, b3, c3, d3) 3 weeks.

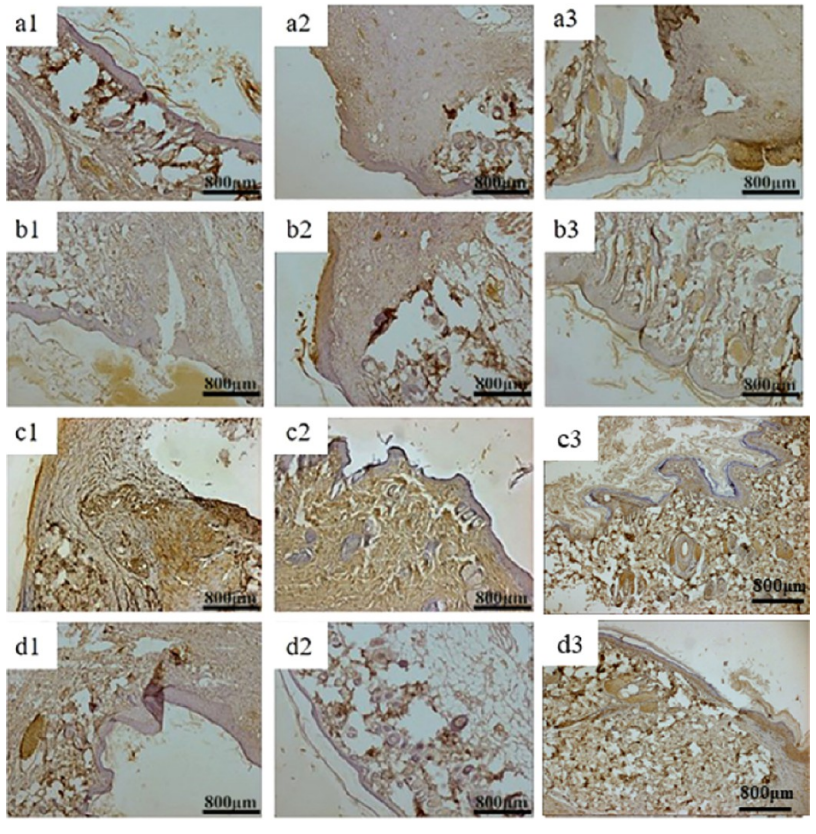

Figure 14. bFGF immunohistochemical analysis of wound areas treated with four kinds collagen-based scaffolds (a) blank group, (b) GA-pADM group, (c) pADM group, (d) QCT−TTO−pADM group; (a1, b1, c1, d1) 1 week; (a2, b2, c2, d2) 2 weeks; (a3, b3, c3, d3) 3 weeks.

https://dx.doi.org/10.1021/acsomega.0c01940
ACS Omega 2020, 5, 20238−20249

tissues. However, glutaraldehyde may introduce some toxicity to materials, which may cause poor biocompatibility. After 3 weeks, the positive expression of PDGF was found in hair follicles and epidermis cells in the dermis, indicating that PDGF had the potential to promote the proliferation and growth of epithelium.[58] As shown in Figure 14, the expression of bFGF was positive in the whole process of wound healing. In the first week of wound healing, bFGF may be related to the formation of wound capillaries and the growth of fibroblasts.[59] In the second week of wound healing, bFGF appeared in the new epidermis, which revealed that bFGF might have the ability to promote the proliferation and regeneration of epidermis cells. At the third week of wound healing, the expression of bFGF was much higher, which may be related to the proliferation of scar tissue and the formation of small vessels in the dermis.

In conclusion, QCT−TTO−pADM was able to promote the expression of bFGF, VEGF, and PDGF in the process of skin wound healing, and it was superior to GA-pADM and pADM in wound healing.

3. CONCLUSIONS

By adding natural plant antimicrobial TTO, pADM was given excellent antibacterial property. The thermal stability, mechanical properties, resistance to enzyme, and hydrophilicity of pADM were totally improved by adding the natural cross-linking agent QCT. It was proved that QCT−TTO−pADM had good biocompatibility in vitro and in vivo and could effectively promote wound repair and even prevent the infection. In conclusion, it was confirmed that QCT and TTO could be used extensively in the modification of medical collagen materials, which provided a method for producing an antibacterial medical material with good performance.

4. MATERIALS AND METHODS

4.1. Materials. pADM was prepared strictly according to our previous work and patent ZL200410022506.9.[53] QCT and TTO were obtained from Sinopharm Group Co., Ltd (Shanghai, China). Bacterial collagenase type I was obtained from Sigma-Aldrich (St. Louis, MO). Calf serum was purchased from Shanghai Fumeng Gene Biotechnology co., Ltd (Shanghai, China). Mouse fibroblast L929 was supplied by Shanghai Bioleaf Biotech Co., Ltd (Shanghai, China). RPMI 1640 medium, antibiotic solution, 3-(4,5-dimethylthiazol-2-yl)-2,5-diphenyltetrazolium bromide, and trypsin were purchased from Thermo Fisher Scientific Inc (Beijing, China). Other chemicals and reagents were purchased from Kelong Chemical Reagent Co., Ltd. (Chengdu, China), if not specifically mentioned.

4.2. Treatment of pADM. At first, 400 mg of QCT was dissolved in 20 mL of ethanol. A homogeneous solution was obtained after ultrasonic treatment for 15 min. Subsequently, different amounts of the QCT solution were respectively added to achieve concentrations of 1, 2.5, 5, 10, and 20. Then, 2 g of pADM and TTO (25% w/w, the dosage has been optimized in our previous work) were added into the solution. After that, under the condition of continuous shaking at 37 °C, cross-linking was performed for 24 h. Finally, each sample was washed using ultrapure water for five times, and then lyophilized before testing.[53] GA-pADM was used as the control during in vivo evaluation.

4.3. FTIR Spectroscopy. Samples (2 mg) were ground with 100 mg of potassium bromide (KBr) and then compressed into a flake. FTIR spectra of the materials were collected by an FTIR spectrometer (MAGNA IR560, Nicolet, America) in the range of 4000−400 cm^{-1} at 25 °C. The scanning rate was set at 32 scans per spectrum.

4.4. DSC Analysis. The thermal denaturation temperature of pADM and QCT−TTO−pADM was determined by a differential scanning calorimeter (DSC-200PC PHOX, Netzsch, Germany) equipped with the Netzsch Proteus analysis software.[60] Using an empty pan as a reference, 5 mg of samples were sealed in the aluminum pans and further scanned under a nitrogen flow of 60 mL/min. The temperature went from 10 to 120 °C. The heating rate was set at 10 °C/min

4.5. TG Analysis. pADM and QCT−TTO−pADM (approximately 5 mg) were, respectively, tested on a thermogravimetric analyzer (Netzsch TG 209, Germany) to record the mass change of materials, heated from 50 to 800 °C at a heating rate of 20 °C/min. The test was taken under a nitrogen atmosphere.

4.6. Mechanical Characterization. After 48 h of air adjustment, the tensile strength and elongation at break of the rectangular samples were measured by a universal testing machine (GT-AI-7000S, Gotech, China) at a rate of 100 mm/min. Each set of data consisted of three parallel samples.

4.7. In Vitro Enzymatic Degradation. Dry pADM materials were cut into square pieces and weighed (denoted as W_1). Five milliliters collagenase type I/PBS solution (5 U/mL, 3 mL/mg sample) was, respectively, added to each group for 28 days at 37 °C. The solution was changed every other day. On days 1, 2, 5, 9, 13, 20, and 28, the materials were removed from the solution, washed five times with distilled water, then lyophilized, and weighed (W_2). The degradation rate was calculated by the following equation[61]

$$\text{degradation rate}\ (\%) = [(W_1 - W_2)/W_1] \times 100\% \quad (1)$$

4.8. Micromorphology Analysis. A certain amount of QCT−TTO−pADM was taken, dipped in liquid nitrogen, and then broken off. The section was treated with gold spraying. The samples were placed under a scanning electron microscope (SEM, Hitachi model S520, Japan) under the condition of 20 kV acceleration voltage for magnified observation.

4.9. Contact Angle (CA) Detection. A video contact angle tester (OCA-H200, Data-physics, Germany) was used to detect the hydrophilicity of pADM and QCT−TTO−pADM. At least five different surface areas were measured for each sample. Finally, the average contact angle was obtained.

4.10. Bactericidal Activity Tests. In this research, the samples were handled with *S. aureus* (gram-positive bacteria) and *E. coli* (gram-negative bacteria) to evaluate the bactericidal activity.

All of the samples were irradiated under ^{60}Co irradiation in advance. A bacterial suspension with the concentration of 10^5 CFU/mL was prepared to evaluate the bacteria-killing ratio.[62] The bacteria-killing ratio was tested by incubating bacteria for 48 h and then counting live bacteria according to a dilution-plate method.[61] The live bacteria number of the control group was designated as N_0 and that of the samples was designated as N_{sample}. The antibacterial rates of the materials were calculated by the following equation[63]

$$\text{antibacterial rate}\ (\%) = (N_0 - N_{sample}) \times 100\%\ /N_0 \quad (2)$$

https://dx.doi.org/10.1021/acsomega.0c01940
ACS Omega 2020, 5, 20238−20249

4.11. Cytocompatibility Studies. The cytotoxicity of the materials was determined by the MTT method.[64] Cells were seeded onto samples at a density of 1×10^4 per milliliter, and then incubated for 1, 3, and 5 days. The optical density (OD) was measured with a microplate reader (model 550, Bio Rad Corp., America) at a wavelength of 492 nm.[60] The states of the mouse fibroblast L929 on different samples were analyzed by an inverted optical microscope. The relative growth rate (RGR) of the materials was calculated by the eq 3

$$\text{RGR}\ (\%) = (\text{the OD value of samples} / \text{the OD value of control}) \times 100\% \quad (3)$$

4.12. In Vivo Study. The animal experiments of this project were completed in the Animal Experiment Center of Sichuan University. All animals were handled according to the National Institutes of Health Guide for the Care and Use of Laboratory Animals (NIH Publications No. 8023, revised 1978). All operations on animals were approved by the Sichuan University Animal Care and Use Committee.

Thirty SD rats weighing 300−500 g were taken and divided into three groups (pADM group, GA-pADM group, and QCT−TTO−pADM group). After anesthesia, the rats were shaved and disinfected. Full-thickness skin wounds of 1 cm × 2 cm were made on each side of the rat spine. Then, all samples were applied on the right side of the injury while nothing was on left as a control group. After operation, the rats were sent to animal house for single cage feeding freely. The SD rats were given penicillin injections for every 3 days. The activity of rats and wound dressing were observed every day. The rats were killed in batches at 1, 2, or 3 weeks after operation. The wounds and peripheral tissues were washed with normal saline and fixed in paraformaldehyde for 2 days, then handled with alcohol gradient dehydration. Finally, tissues were embedded in paraffin for histopathological staining and observation.

4.13. Statistics. Statistical analysis of MTT results was handled on SPSS 19.0. A value corresponding to $*p < 0.05$ was considered as statistically significant.

AUTHOR INFORMATION

Corresponding Authors

Nianhua Dan − *College of Biomass Science and Engineering, Research Center of Biomedical Engineering, and Key Laboratory for Leather Chemistry and Engineering of the Education Ministry, Sichuan University, Chengdu, Sichuan 610065, China*; Email: dannianhua@scu.edu.cn

Weihua Dan − *College of Biomass Science and Engineering, Research Center of Biomedical Engineering, and Key Laboratory for Leather Chemistry and Engineering of the Education Ministry, Sichuan University, Chengdu, Sichuan 610065, China*; orcid.org/0000-0002-2111-0634; Phone: +86 28 85408988; Email: danweihua_scu@126.com

Authors

Lu Wang − *College of Biomass Science and Engineering, Research Center of Biomedical Engineering, and Key Laboratory for Leather Chemistry and Engineering of the Education Ministry, Sichuan University, Chengdu, Sichuan 610065, China*

Juxia Gong − *College of Biomass Science and Engineering, Research Center of Biomedical Engineering, and Key Laboratory for Leather Chemistry and Engineering of the Education Ministry, Sichuan University, Chengdu, Sichuan 610065, China*

Ye Dan − *School of Manufacturing Science and Engineering, Sichuan University, Chengdu, Sichuan 610065, China*

Yanping Huang − *College of Biomass Science and Engineering, Research Center of Biomedical Engineering, and Key Laboratory for Leather Chemistry and Engineering of the Education Ministry, Sichuan University, Chengdu, Sichuan 610065, China*

Complete contact information is available at: https://pubs.acs.org/10.1021/acsomega.0c01940

Notes

The authors declare no competing financial interest.

ACKNOWLEDGMENTS

We thank the Fundamental Research Funds for the Central Universities [grant number 20826041C4159] and the National Natural Science Foundation of China [grant number 51473001]. We thank our lab members for their help during experiments.

REFERENCES

(1) Wuthisuthimethawee, P.; Lindquist, S. J.; Sandler, N.; Clavisi, O.; Korin, S.; Watters, D.; Gruen, R. L. Wound Management in Disaster Settings. *World J. Surg.* **2015**, *39*, 842−853.

(2) Zhong, W. Efficacy and toxicity of antibacterial agents used in wound dressings. *Cutaneous Ocul. Toxicol.* **2015**, *34*, 61−67.

(3) Sutjarittangtham, K.; Sanpa, S.; Tunkasiri, T.; Chantawannakul, P.; Intatha, U.; Eitssayeam, S. Bactericidal effects of propolis/polylactic acid (PLA) nanofibres obtained via electrospinning. *J. Apic. Res.* **2014**, *53*, 109−115.

(4) Pabst, A. M.; Lehmann, K.-M.; Walter, C.; Krueger, M.; Stratul, S.-I.; Kasaj, A. Influence of porcine-derived collagen matrix on endothelial progenitor cells: an in vitro study. *Odontology* **2016**, *104*, 19−26.

(5) Yang, M. Y.; Zhou, G. S.; Castano-Izquierdo, H.; Zhu, Y.; Mao, C. B. Biomineralization of Natural Collagenous Nanofibrous Membranes and Their Potential Use in Bone Tissue Engineering. *J. Biomed. Nanotechnol.* **2015**, *11*, 447−456.

(6) Park, J. Y.; Song, B. R.; Lee, J. W.; Park, S. H.; Kang, T. W.; Yun, H. W.; Park, S. H.; Min, B. H.; Kim, M. S. Preparation of a Cross-Linked Cartilage Acellular-Matrix Film and Its In Vivo Evaluation as an Antiadhesive Barrier. *Polymers* **2019**, No. 247.

(7) Hille-Betz, U.; Kniebusch, N.; Wojcinski, S.; Henseler, H.; Heyl, V.; Ohlinger, R.; Paepke, S.; Klapdor, R.; Krause-Bergmann, B. Breast Reconstruction and Revision Surgery for Implant-associated Breast Deformities Using Porcine Acellular Dermal Matrix: A Multicenter Study of 156 Cases. *J. Surg. Oncol.* **2015**, *22*, 1146−1152.

(8) Fang, Q.; Gu, T. X.; Fan, J.; Zhang, Y. M.; Wang, Y. C.; Zhao, Y.; Zhao, P. Evaluation of a hybrid small caliber vascular graft in a rabbit model. *J. Thorac. Cardiovasc. Surg.* **2020**, *159*, 461−473.

(9) Han, B. S.; Xue, F.; Fan, C. Y.; Mo, X. M. Surface heparinization and blood compatibility modification of small intestinal submucosa (SIS) for small-caliber vascular regeneration. *Bio-Med. Mater. Eng.* **2017**, *28*, 213−222.

(10) Martin, C.; Low, W. L.; Amin, M. C. I. M.; Radecka, I.; Raj, P.; Kenward, K. Current trends in the development of wound dressings, biomaterials and devices. *Pharm. Pat. Anal.* **2013**, *2*, 341−359.

(11) Heine, J.; Schmiedl, A.; Cebotari, S.; Karck, M.; Mertsching, H.; Haverich, A.; Kallenbach, K. Tissue Engineering Human Small-Caliber Autologous Vessels Using a Xenogenous Decellularized Connective Tissue Matrix Approach: Preclinical Comparative Biomechanical Studies. *Artif. Organs* **2011**, *35*, 930−940.

(12) Reichling, J.; Landvatter, U.; Wagner, H.; Kostka, K.-H.; Schaefer, U. F. In vitro studies on release and human skin permeation of Australian tea tree oil (TTO) from topical formulations. *Eur. J. Pharm. Biopharm.* **2006**, *64*, 222−228.

(13) Giordani, C.; Molinari, A.; Toccacieli, L.; Calcabrini, A.; Stringaro, A.; Chistolini, P.; Arancia, G.; Diociaiuti, M. Interaction of tea tree oil with model and cellular membranes. *J. Med. Chem.* **2006**, *49*, 4581−4588.
(14) Oliva, A.; Costantini, S.; De Angelis, M.; Garzoli, S.; Bozovic, M.; Mascellino, M. T.; Vullo, V.; Ragno, R. High Potency of *Melaleuca alternifolia* Essential Oil against Multi-Drug Resistant Gram-Negative Bacteria and Methicillin-Resistant *Staphylococcus aureus*. *Molecules* **2018**, *23*, No. 2584.
(15) Lin, G.; Chen, H.; Zhou, H.; Zhou, X.; Xu, H. Preparation of Tea Tree Oil/Poly(styrene-butyl methacrylate) Microspheres with Sustained Release and Anti-Bacterial Properties. *Materials* **2018**, *11*, No. 710.
(16) de Groot, A. C.; Schmidt, E. Tea tree oil: contact allergy and chemical composition. *Contact Dermatitis* **2016**, *75*, 129−143.
(17) Huynh, Q.; Phan, T. D.; Thieu, V. Q. Q.; Tran, S. T.; Do, S. H.; Sandhu, A. In *Extraction and Refining of Essential Oil from Australian Tea Tree, Melaleuca alterfornia, and the Antimicrobial Activity in Cosmetic Products*, Asia-Pacific Interdisciplinary Research Conference, 2012; p 352.
(18) Sánchez-González, L.; Cháfer, M.; Hernández, M.; Chiralt, A.; González-Martínez, C. Antimicrobial activity of polysaccharide films containing essential oils. *Food Control* **2011**, *22*, 1302−1310.
(19) Chen, Y.; Dan, N.; Dan, W.; Yu, G. Supercritical CO2 fluid-assisted cross-linking of porcine acellular dermal matrix by ethylene glycol diglycidyl ether. *J. CO2 Util.* **2018**, *25*, 264−274.
(20) Hu, Y.; Liu, L.; Dan, W.; Dan, N.; Gu, Z.; Yu, X. Synergistic effect of carbodiimide and dehydrothermal crosslinking on acellular dermal matrix. *Int. J. Biol. Macromol.* **2013**, *55*, 221−230.
(21) Hu, Y.; Dan, W.; Xiong, S.; Kang, Y.; Dhinakar, A.; Wu, J.; Gu, Z. Development of collagen/polydopamine complexed matrix as mechanically enhanced and highly biocompatible semi-natural tissue engineering scaffold. *Acta Biomater.* **2017**, *47*, 135−148.
(22) Zhu, S.; Gu, Z.; Hu, Y.; Dan, W.; Xiong, S. Evaluation of alginate dialdehyde as a suitable crosslinker on modifying porcine acellular dermal matrix: The aggregation of collagenous fibers. *J. Appl. Polym. Sci.* **2016**, *133*, No. 43550.
(23) Xiao, S.; Tang, G.; Dan, N.; Dan, W. Study on the Crosslinked acellular Porcine dermis Matrix with procyanidins. *Leather Sci. Eng.* **2012**, *22*, 15−19.
(24) Li, Y.; Yao, J.; Han, C.; Yang, J.; Chaudhry, M. T.; Wang, S.; Liu, H.; Yin, Y. Quercetin, Inflammation and Immunity. *Nutrients* **2016**, *8*, No. 167.
(25) Davis, J. M.; Murphy, E. A.; Carmichael, M. D. Effects of the Dietary Flavonoid Quercetin Upon Performance and Health. *Nutr. Ergogenic Aids* **2009**, *8*, 206−213.
(26) Chirumbolo, S. The role of quercetin, flavonols and flavones in modulating inflammatory cell function Inflammation Allergy. *Drug Targets* **2010**, *9*, 263−285.
(27) Zhai, W. Y.; Lu, X. Q.; Chang, J.; Zhou, Y. L.; Zhang, H. F. Quercetin-crosslinked porcine heart valve matrix: Mechanical properties, stability, anticalcification and cytocompatibility. *Acta Biomater.* **2010**, *6*, 389−395.
(28) Zhai, W. Y.; Lu, X. Q.; Chang, J.; Zhou, Y. L.; Zhang, H. F. Quercetin-crosslinked porcine heart valve matrix: Mechanical properties, stability, anticalcification and cytocompatibility. *Acta Biomater.* **2010**, *6*, 389−395.
(29) Liu, X.; Dan, N.; Dan, W. Preparation and characterization of an advanced collagen aggregate from porcine acellular dermal matrix. *Int. J. Biol. Macromol.* **2016**, *88*, 179−188.
(30) Riaz, T.; Zeeshan, R.; Zarif, F.; Ilyas, K.; Muhammad, N.; Safi, S. Z.; Rahim, A.; Rizvi, S. A. A.; Rehman, I. U. FTIR analysis of natural and synthetic collagen. *Appl. Spectrosc. Rev.* **2018**, *53*, 703−746.
(31) Krimm, S.; Bandekar, J. Vibrational Spectroscopy and Conformation of Peptides, Polypeptides, and Proteins. *Adv. Protein Chem.* **1986**, *38*, 181−364.
(32) Kittiphattanabawon, P.; Benjakul, S.; Visessanguan, W.; Kishimura, H.; Shahidi, F. Isolation and Characterisation of collagen from the East China normal University skin of brownbanded bamboo shark (*Chiloscyllium punctatum*). *Food Chem.* **2010**, *119*, 1519−1526.
(33) Chavoshpour-Natanzi, Z.; Sahihi, M. Encapsulation of quercetin-loaded beta-lactoglobulin for drug delivery using modified anti-solvent method. *Food Hydrocolloids* **2019**, *96*, 493−502.
(34) Mohammadian, M.; Moghaddam, A. D.; Sharifan, A.; Dabaghi, P.; Hadi, S. Nanocomplexes of whey protein fibrillar aggregates and quercetin as novel multi-functional biopolymeric ingredients: interaction, chemical structure, and bio-functionality. *J. Iran. Chem. Soc.* **2020**, 1−12.
(35) Rastian, Z.; Puetz, S.; Wang, Y.; Kumar, S.; Fleissner, F.; Weidner, T.; Parekh, S. H. Type I Collagen from Jellyfish *Catostylus mosaicus* for Biomaterial Applications. *ACS Biomater. Sci. Eng.* **2018**, *4*, 2115−2125.
(36) Zhang, C.; Yang, X.; Hu, W.; Han, X.; Fan, L.; Tao, S. Preparation and characterization of carboxymethyl chitosan/collagen peptide/oxidized konjac composite hydrogel. *Int. J. Biol. Macromol.* **2020**, *149*, 31−40.
(37) Liu, X. H.; Zheng, S. D.; Dan, W. H.; Dan, N. H. Ultrasound-mediated Preparation and Evaluation of a Collagen/PVP-PCL Micro- and Nanofiber Scaffold Electrospun from Chloroform/Ethanol Mixture. *Fibers Polym.* **2016**, *17*, 1186−1197.
(38) Hu, Y.; Lju, L.; Gu, Z.; Dan, W.; Dan, N.; Yu, X. Modification of collagen with a natural derived cross-linker, alginate dialdehyde. *Carbohydr. Polym.* **2014**, *102*, 324−332.
(39) Dan, W.; Chen, Y.; Dan, N.; Zheng, X.; Wang, L.; Yang, C.; Huang, Y.; Liu, X.; Hu, Y. Multi-level collagen aggregates and their applications in biomedical applications. *Int. J. Polym. Anal. Charact.* **2019**, *24*, 667−683.
(40) Horn, M. M.; Martins, V. C. A.; Plepis, A. M. D. Interaction of anionic collagen with chitosan: Effect on thermal and morphological characteristics. *Carbohydr. Polym.* **2009**, *77*, 239−243.
(41) Liu, X.; Zheng, M.; Wang, X.; Luo, X.; Hou, M.; Yue, O. Biofabrication and Characterization of Collagens with Different Hierarchical Architectures. *ACS Biomater. Sci. Eng.* **2020**, *6*, 739−748.
(42) Chen, Y.; Dan, N.; Wang, L.; Liu, X.; Dan, W. Study on the cross-linking effect of a natural derived oxidized chitosan oligosaccharide on the porcine acellular dermal matrix. *RSC Adv.* **2016**, *6*, 38052−38063.
(43) Jiang, H.; Zheng, M.; Liu, X.; Zhang, S.; Wang, X.; Chen, Y.; Hou, M.; Zhu, J. Feasibility Study of Tissue Transglutaminase for Self-Catalytic Cross-Linking of Self-Assembled Collagen Fibril Hydrogel and Its Promising Application in Wound Healing Promotion. *ACS Omega* **2019**, *4*, 12606−12615.
(44) Hasan, A.; Saxena, V.; Pandey, L. M. Surface Functionalization of Ti6Al4V via Self-assembled Monolayers for Improved Protein Adsorption and Fibroblast Adhesion. *Langmuir* **2018**, *34*, 3494−3506.
(45) Liu, X. H.; Yan, Z. A.; Wang, X. C.; Luo, X. M.; Qiang, T. T.; Dan, W. H. Development of a Novel Collagenous Matrix Based on Tissue-Mimicking Advanced Collagen Aggregate Synthetically Cross-Linked with Biological Cross-Linkers, OCS, and beta-ODAP for Wound Healing. *ACS Sustainable Chem. Eng.* **2018**, *6*, 17142−17151.
(46) Madhurakkat Perikamana, S. K.; Lee, J.; Lee, Y. B.; Shin, Y. M.; Lee, E. J.; Mikos, A. G.; Shin, H. Materials from Mussel-Inspired Chemistry for Cell and Tissue Engineering Applications. *Biomacromolecules* **2015**, *16*, 2541−2555.
(47) Sikkema, J.; Debont, J. A. M.; Poolman, B. Mechanisms of membrane toxicity of hydrocarbons. *Microbiol. Rev.* **1995**, *59*, 201−222.
(48) Sun, L. M.; Zhang, C. L.; Li, P. Characterization, Antibiofilm, and Mechanism of Action of Novel PEG-Stabilized Lipid Nanoparticles Loaded with Terpinen-4-ol. *J. Agric. Food Chem.* **2012**, *60*, 6150−6156.
(49) Lu, D.; Wang, H.; Li, Te.; Li, Y.; Wang, X.; Niu, P.; Guo, H.; Sun, S.; Wang, X.; Guan, X.; Ma, H.; Lei, Z. Versatile Surgical Adhesive and Hemostatic Materials: Synthesis, Properties, and Application of Thermoresponsive Polypeptides. *Chem. Mater.* **2017**, *29*, 5493−5503.

https://dx.doi.org/10.1021/acsomega.0c01940
ACS Omega 2020, 5, 20238−20249

(50) Yang, L.; Li, X. F.; Wang, D. M.; Mu, S. F.; Lv, W. H.; Hao, Y. W.; Lu, X. S.; Zhang, G. J.; Nan, W. B.; Chen, H. L.; Xie, L. Q.; Zhang, Y. J.; Dong, Y. Z.; Zhang, Q. Q.; Zhao, L. Improved mechanical properties by modifying fibrin scaffold with PCL and its biocompatibility evaluation. *J. Biomater. Sci., Polym. Ed.* **2020**, *31*, 658−678.
(51) Zhao, Y.; Li, Z. H.; Song, S. L.; Yang, K. R.; Liu, H.; Yang, Z.; Wang, J. C.; Yang, B.; Lin, Q. Skin-Inspired Antibacterial Conductive Hydrogels for Epidermal Sensors and Diabetic Foot Wound Dressings. *Adv. Funct. Mater.* **2019**, *29*, No. 1901474.
(52) Ramanathan, G.; Singaravelu, S.; Muthukumar, T.; Thyagarajan, S.; Perumal, P. T.; Sivagnanam, U. T. Design and characterization of 3D hybrid collagen matrixes as a dermal substitute in skin tissue engineering. *Mater. Sci. Eng., C* **2017**, *72*, 359−370.
(53) Chen, Y.; Dan, N.; Dan, W.; Liu, X.; Cong, L. A novel antibacterial acellular porcine dermal matrix cross-linked with oxidized chitosan oligosaccharide and modified by in situ synthesis of silver nanoparticles for wound healing applications. *Mater. Sci. Eng., C* **2019**, *94*, 1020−1036.
(54) Yang, B.; Zhou, L.; Peng, B.; Sun, Z.; Dai, Y.; Zheng, J. In vitro comparative evaluation of recombinant growth factors for tissue engineering of bladder in patients with neurogenic bladder. *J. Surg. Res.* **2014**, *186*, 63−72.
(55) Gallego-Muñoz, P.; Ibares-Frias, L.; Cruz Valsero-Blanco, M.; Cantalapiedra-Rodriguez, R.; Merayo-Lloves, J.; Carmen Martinez-Garcia, M. Effects of TGF β 1, PDGF-BB, and bFGF, on human corneal fibroblasts proliferation and differentiation during stromal repair. *Cytokine* **2017**, *96*, 94−101.
(56) Cheng, T. L.; Chen, P. K.; Huang, W. K.; Kuo, C. H.; Cho, C. F.; Wang, K. C.; Shi, G. Y.; Wu, H. L.; Lai, C. H. Plasminogen/thrombomodulin signaling enhances VEGF expression to promote cutaneous wound healing. *J. Mol. Med.* **2018**, *96*, 1333−1344.
(57) Zheng, C.; Liu, X. H.; Luo, X. M.; Zheng, M. H.; Wang, X. C.; Dan, W. H.; Jiang, H. E. Development of a novel bio-inspired "cotton-like" collagen aggregate/chitin based biomaterial with a biomimetic 3D microstructure for efficient hemostasis and tissue repair. *J. Mater. Chem. B* **2019**, *7*, 7338−7350.
(58) Hanafiah, O. A.; Poravi, R.; Angga, D.; Abidin, T.; Ilyas, S.; Nainggolan, M.; Syamsudin, E. In *The Role of TGFβ 1 and PDGF BB in Wound Healing of the Palate*, International Dental Conference of Sumatera Utara 2017 (IDCSU 2017); Atlantis Press, 2017; pp 219−225.
(59) Zhang, X.; Kang, X.; Jin, L.; Bai, J.; Liu, W.; Wang, Z. Stimulation of wound healing using bioinspired hydrogels with basic fibroblast growth factor (bFGF). *Int. J. Nanomed.* **2018**, *13*, 3897−3906.
(60) Liu, T.; Shi, L.; Gu, Z.; Dan, W.; Dan, N. A novel combined polyphenol-aldehyde crosslinking of collagen film-Applications in biomedical materials. *Int. J. Biol. Macromol.* **2017**, *101*, 889−895.
(61) Chen, Y. N.; Dan, N. H.; Dan, W. H.; Liu, X. H.; Cong, L. L. A novel antibacterial acellular porcine dermal matrix cross-linked with oxidized chitosan oligosaccharide and modified by in situ synthesis of silver nanoparticles for wound healing applications. *Mater. Sci. Eng., C* **2019**, *94*, 1020−1036.
(62) Huang, Y.; Dan, N.; Dan, W.; Zhao, W.; Bai, Z.; Chen, Y.; Yang, C. Facile fabrication of gelatin and polycaprolactone based bilayered membranes via spin coating method with antibacterial and cyto-compatible properties. *Int. J. Biol. Macromol.* **2019**, *124*, 699−707.
(63) Chen, Y. N.; Dan, N. H.; Huang, Y. P.; Bai, Z. X.; Yang, C. K.; Dan, W. H.; Cong, L. L. Functional chemical modification of a porcine acellular dermal matrix with a modified naturally derived polysaccharide crosslinker. *J. Appl. Polym. Sci.* **2019**, *136*, No. 47633.
(64) Huang, Y.; Dan, N.; Dan, W.; Zhao, W.; Bai, Z.; Chen, Y.; Yang, C. Bilayered Antimicrobial Nanofiber Membranes for Wound Dressings via in Situ Cross-Linking Polymerization and Electrospinning. *Ind. Eng. Chem. Res.* **2018**, *57*, 17048−17057.

https://dx.doi.org/10.1021/acsomega.0c01940
ACS Omega 2020, 5, 20238−20249